



14 **ABSTRACT**

15

16 The ongoing process of global urbanization contributes to an increase in stormwater runoff from  
17 impervious surfaces, threatening also water quality. Green roofs have been proved to be innovative  
18 stormwater management measures to partially restore natural states, enhancing interception,  
19 infiltration and evapotranspiration fluxes. The amount of water that is retained within green roofs  
20 depends not only on their depth, but also on the climate, which drives the stochastic soil moisture  
21 dynamic. In this context, a simple tool for assessing performances of green roofs worldwide in  
22 terms of retained water is still missing and highly desirable for practical assessments.

23 The aim of this work is to explore retention performances of green roofs as a function of their  
24 depth and in different climate regimes. Two soil depths are investigated, one representing the  
25 intensive usual configuration and another representing the extensive one. The role of the climate in  
26 driving water retention has been represented by rainfall and potential evapotranspiration dynamics.  
27 A simple conceptual weather generator has been implemented and used for stochastic simulation of  
28 daily rainfall and potential evapotranspiration. Stochastic forcing is used as an input of a simple  
29 conceptual hydrological model for estimating long-term water partitioning between rainfall, runoff  
30 and actual evapotranspiration. Coupling the stochastic weather generator with the conceptual  
31 hydrological model, we assessed the amount of rainfall diverted into evapotranspiration for  
32 different combinations of annual rainfall and potential evapotranspiration in five representative  
33 climatic regimes. Results quantified the capabilities of green roofs in retaining rainfall and  
34 consequently in reducing discharges into sewer systems at an annual time scale. The role of  
35 substrate depth has been recognized to be crucial in determining green roof retention performances,  
36 which in general increase from extensive to intensive settings. Looking at the role of climatic  
37 conditions, namely annual rainfall, potential evapotranspiration and their seasonality cycles, we  
38 found that they drive green roof retention performances, which are the maxima when rainfall and  
39 temperature are in phase.

40 Finally, we provide design charts for a first approximation of possible hydrological benefits  
41 deriving from the implementation of intensive or extensive green roofs in different world areas. As  
42 an example, 25 big cities have been indicated as benchmark case studies.

43

44

## 45 **1. Introduction**

46 The continuous growth of impervious surface areas leads to increased downstream flows with  
47 critical consequences for the functioning of existing sewer systems and triggers water quality  
48 degradation in receiving water bodies (Carter and Jackson, 2007; Carter and Rasmussen, 2006). A  
49 variety of management practices have been proposed to limit the environmental pressures  
50 associated with the altered hydrology of urban areas. In this context, green roofs are an innovative  
51 solution for mitigation of the impact of stormwater runoff, with the advantage of recovering green  
52 spaces, while preserving environmental quality (Getter and Rowe, 2006). Green roofs are indeed a  
53 valid alternative to traditional stormwater design and a low impact development practice (Dietz,  
54 2007). Several authors recommend the use of vegetative roofs as an attractive stormwater  
55 management practice in urban watersheds, in order to reproduce the benefits produced by the  
56 interception and evapotranspiration processes in the natural water cycle, as in less disturbed  
57 environments. Green roofs are now quite familiar in Europe and North America: some cities have  
58 built green roof pilot projects and adopted incentives for applying green roof practices (Dvorak and  
59 Volder, 2010), while standards and guidelines are also being set up.

60 Several environmental benefits can be associated with green roofs, mainly related to the  
61 reduction of building energy consumption, mitigation of urban heat island effect, improvement of  
62 air quality, water management, increase of sound insulation, and ecological preservation (Berardi  
63 and Ghaffarian Hoseini, 2014). An important benefit related to green roofs is that they can  
64 efficiently detain and retain stormwater when compared to conventional roofs. In the following we

65 analyze some scientific studies aimed at the evaluation of hydrological performances of green roofs  
66 by distinguishing between field experiments and modelling approaches.

67 Many field experiments have been carried out in order to understand the hydrological behaviour  
68 of green roofs and to quantify the water-related benefits in specific climatic and physical  
69 conditions. An interesting case has been proposed by Carter and Rasmussen (2006): a paired green  
70 roof-black roof test plot was constructed at the University of Georgia (USA) and monitored for one  
71 year for the effectiveness of the green roof in reducing stormwater flows. Green roof precipitation  
72 retention decreased with precipitation depth; ranging from about 90 percent for small storms to  
73 slightly less than 50 percent for larger storms. Moreover, they also found that runoff from the green  
74 roof was delayed and that the average runoff lag times increased.

75 Bengtsson et al. (2005) studied a thin extensive green roof and its water balance in southern  
76 Sweden. They observed that runoff from the green roof is substantially reduced when compared to  
77 the runoff from black roofs because of evapotranspiration. As a physical interpretation of the water  
78 dynamics within the green roof, they associated the beginning of runoff with the condition of soil  
79 moisture reaching or exceeding the field capacity, and estimated the consequent runoff as equal to  
80 the precipitation excess. They argued that the daily runoff dynamics could be described as a  
81 function of daily precipitation, potential evaporation and storage capacity of the green roof.

82 Czemieli Berndtsson (2010) made a critical review of green roof performances on the basis of  
83 results from full-scale installations as well as from laboratory models and looked for factors  
84 affecting runoff dynamics. He concluded that geometrical properties (mainly slope), climate  
85 (mainly rainfall) and vegetation (its age) are fundamental in determining runoff from green roofs.

86 Feng et al. (2010) quantified the energy balance components within an extensive green roof  
87 installation in the South China University of Technology in Guangzhou (China). They found that,  
88 without water limitations, incoming solar radiation was diverted into evapotranspiration of the  
89 plant-soil system (60%), long-wave radiation exchange between the canopy and the atmosphere  
90 (30%) and net photosynthesis of plants (10%).

91 Performances of green roofs have been also investigated in the Mediterranean climate by Fioretti  
92 et al. (2010) with two full-scale experiments in north-west and central Italy. They concluded that  
93 green roofs significantly mitigate storm water runoff generation in terms of runoff volume  
94 reduction, peak attenuation and increase of concentration time, although reduced performance  
95 could be observed during high precipitation periods. Under sub-tropical climate conditions, Voyde  
96 et al. (2010) analyzed field monitoring results from a large extensive green roof in Auckland, New  
97 Zealand (NZ). They found that the green roof retained about 82% of rainfall received per rainfall  
98 event, with a median peak flow reduction of 93% compared to rainfall intensity. Similarly to other  
99 studies, also Voyde et al. (2010) individuated in rain depth, rain intensity, climatic variables and  
100 antecedent dry days the main key factors influencing the hydrology of green roofs.

101 DeNardo et al. (2005) studied a green flat roof at Rock Springs, Pennsylvania (USA). They  
102 observed a range of rainfall retention from 19% to 98% in seven storms and peak runoff delayed by  
103 2 hours. The effect of slope on extensive green roof stormwater retention was instead analyzed by  
104 Getter et al. (2007) using 12 extensive green roof platforms constructed at the Michigan State  
105 University (USA). They demonstrated that the lower the slope the higher the retention, with an  
106 average retention value of about 80%.

107 Monterusso et al. (2004) analyzed runoff from four commercial green roof systems containing  
108 three distinct vegetation types at the Michigan State University (USA). Rainfall retained during  
109 their experiments ranged from 39% to 58%. It is worth noticing that their results highlight how  
110 differences in water retention can be attributed to substrate depth, rather than drainage system or  
111 vegetation type.

112 Two studies made in the UK by Stovin (2010) and Stovin et al. (2012) demonstrated the  
113 important role of mean rainfall intensity, rainfall depth and an antecedent dry weather period,  
114 which conditions antecedent moisture conditions. The latter is indeed crucial in determining the  
115 performance of green roofs, in terms of retentions, peak attenuation and delay under extreme  
116 rainfall conditions.

117 If field experiments, as briefly referred to above, allow the underlying physical processes to be  
118 understood, modelling approaches permit phenomena to be mimicked, and consequently to  
119 simulate green roof performances even in unmonitored conditions. Hydrological modelling  
120 demonstrated that widespread green roof implementation can significantly reduce peak runoff rates,  
121 particularly for small storm events (Carter and Jackson, 2007).

122 Hilten et al. (2008) modelled stormwater runoff data from green roofs with the HYDRUS- 1D  
123 model (Šimůnek et al., 2008) in order to determine peak flow, retention and detention time for  
124 runoff. Storm data were collected on a green roof in Athens, Georgia, USA, and used to calibrate  
125 HYDRUS-1D simulated runoff. The study site consisted of a 37 m<sup>2</sup> modular block green roof  
126 containing engineered soil and vegetation including several sedum species. Simulations explicated  
127 the role of rainfall depth in determining water retention: in fact small storms are fully retained  
128 while larger storms are partially attenuated.

129 The work carried out by Palla et al. (2009) advanced the understanding of the unsaturated water  
130 flow in the coarse-grained porous media usually employed in green roofs. Using a bidimensional  
131 model based on Richards' law and the Van Genuchten-Mualem functions they were able to simulate  
132 the variably saturated flow within the green roof system with a satisfactory reproduction of  
133 hydrograph main features, i.e. total discharged volume, peak flow, hydrograph centroid and water  
134 content. In a later study, the same authors compared the performances of HYDRUS-1D with those  
135 obtained by a conceptual linear reservoir in reproducing the hydrologic response of a green roof  
136 system within the urban environment (Palla et al., 2012). They found that, comparing simulations  
137 with observations from a field site in Genova, Italy, the HYDRUS-1D model resulted more  
138 accurate. However, prediction errors of the conceptual model were still limited, so that outflow  
139 hydrographs in terms of both total effluent volume and hydrograph shape were predicted with  
140 acceptable accuracy.

141 While most of the previous mentioned studies focused on event scale or short time windows,  
142 there are few examples in literature of long-term green roof performance evaluations, mainly  
143 approached with hydrological models. An interesting study in this context was proposed by Stovin  
144 et al. (2013). Namely, they used a conceptual hydrological flux model for the long term continuous  
145 simulation of retention performances of extensive green roofs at 4 locations in the UK, with  
146 different annual rainfall (ranging from 500 to 2700 mm/year) and potential evapotranspiration  
147 (from 618 to 700 mm/year). A long term analysis was also performed by Carson et al. (2013) who  
148 simulated extensive green roof performances in NY using an empirical model, calibrated against  
149 observations and forced by historical rainfall (1971-2010). Locatelli et al. (2014) used a  
150 deterministic lumped rainfall–runoff conceptual model to simulate the hydrological response of  
151 green roofs during a 22-year (1989–2010) continuous simulation with Danish climate data. Cipolla  
152 et al. (2016) used field data to calibrate and validate a numerical model, namely the commercial  
153 software SWMM 5.1, to simulate the long-term hydrologic response of an extensive green roof.

154 Although the growing interest in the adoption of green roofs has attracted the attention of many  
155 researchers who focused on the crucial hydrological phenomena emerging from field observations  
156 and the hydrological modeling problem, as briefly reviewed above, many studies were restricted to  
157 specific areas of interest. In this framework, results presented in this manuscript aim to quantify  
158 retention performances of green roofs worldwide, considering several climatic conditions. In order  
159 to do that a simplified stochastic weather generator has been proposed and described in Section 2.1.  
160 This model has been designed to mimic daily rainfall and potential evapotranspiration in different  
161 climates. In particular, it is able to reproduce stationary or seasonal forcings, which in turn have  
162 been used to feed a simple conceptual green roof model, which is described in Section 2.2. The role  
163 of soil substrate in governing water retention at an annual time scale has been investigated  
164 considering an intensive and an extensive configuration. Results have been summarized in Section  
165 3, where design charts for different climatic conditions are also provided for a rapid first  
166 approximation estimate of green roof retention performances worldwide.

## 167 **2. Methods**

### 168 **2.1 Weather generator**

169 The use of a weather generator has always been related to the need of producing indefinitely  
170 long synthetic weather series by simulating key properties of observed meteorological records  
171 (Wilby, 1999). The pioneering idea of using Poisson point process and clustered point processes to  
172 simulate the occurrences of rainfall events at different time scales dates back to the eighties  
173 (Rodríguez-Iturbe et al., 1987a; Rodríguez-Iturbe et al., 1987b). During the last thirty years, in  
174 order to capture and reproduce rainfall properties better across wide ranges of temporal and spatial  
175 scales, there has been considerable research in the field of rainfall modelling using stochastic point  
176 processes, which can be mainly classified as Neyman-Scott and Barlet-Lewis model types (see e.g.  
177 Burlando and Rosso, 1991; Cowpertwait et al., 2002; Cowpertwait et al., 1996; Cowpertwait, 1991;  
178 Cowpertwait and O'Connell, 1997; Entekhabi et al., 1989; Islam et al., 1990; Puente et al., 1993;  
179 Verhoest et al., 1997 among others). Sometimes however, for sake of simplicity or analytical  
180 tractability, the temporal structure within each rain event has been ignored and the marked Poisson  
181 process representing precipitation has been physically interpreted at a daily time scale, where the  
182 pulses of rainfall correspond to daily precipitation assumed to be concentrated at an instant in time  
183 (Laio et al., 2001). We followed this last approach and integrated it with a simple parametric  
184 representation proposed by Milly (1994) to describe the essential features of the annual land surface  
185 hydrologic forcings. The model assumes that the seasonality of climate is mainly driven by the  
186 seasonality of the solar irradiance normal to the top of the atmosphere, which produces a strong  
187 signal with a dominant period of one year in most climatic variables. Precipitation and potential  
188 evapotranspiration time series have been thus simulated as stochastic processes with expected  
189 values modelled with annual harmonics, according to main climatic features observed in 10,000  
190 observational sites worldwide.

191 The occurrence of rainfall  $R$  at time  $t$  is idealized as a series of events at a daily time scale,  
 192 arising from a non-stationary and cyclic Poisson point process with parameter  $1/\lambda$  (rate of the  
 193 Poisson process occurrences, [1/days]) and whose interarrival time  $\lambda(t)$  [days] is here modeled  
 194 through a cyclic sinusoidal function, with 1-year period, according to the following equation:

$$195 \lambda(t) = \bar{\lambda} \left[ 1 + \delta_{\lambda} \sin \left( \frac{2\pi t}{365} + \omega_{\lambda} \right) \right] \quad (1)$$

196 where  $\bar{\lambda}$  is the average interarrival time [days] between rainfall events, the standardized semi-  
 197 amplitude  $\delta_{\lambda}$  is the ratio between the semi-amplitude of the annual harmonics of  $\lambda(t)$  and the  
 198 annual average (i.e.  $\bar{\lambda}$ ), while  $\omega_{\lambda}$  is the initial phase.

199 Rainfall rates during each event are assumed to be a random process described by an exponential  
 200 distribution, with mean  $\alpha(t)$  [mm/day] described as follows:

$$201 \alpha(t) = \bar{\alpha} \left[ 1 + \delta_{\alpha} \sin \left( \frac{2\pi t}{365} + \omega_{\alpha} \right) \right] \quad (2)$$

202 where  $\bar{\alpha}$  is the average amount of rainfall [mm/day], the standardized semi-amplitude  $\delta_{\alpha}$  is the ratio  
 203 of the semi-amplitudes of the annual harmonics of  $\alpha(t)$  to the annual average (i.e.  $\bar{\alpha}$ ), and  $\omega_{\alpha}$  is the  
 204 initial phase.

205 Potential evapotranspiration  $ET_p(t)$  [mm/day] has been modelled with a harmonic as follows:

$$206 ET_p(t) = \overline{ET_p} \left[ 1 + \delta_E \sin \left( \frac{2\pi t}{365} + \omega_E \right) \right] \quad (3)$$

207 where  $\overline{ET_p}$  is the average annual potential evapotranspiration [mm/day], the standardized semi-  
 208 amplitude  $\delta_E$  is the ratios of the semi-amplitude of the annual harmonics of  $ET_p(t)$  to the annual  
 209 average (i.e.  $\overline{ET_p}$ ), and  $\omega_E$  is the initial phase.

210 We decided to reduce the degrees of freedom of this analysis to simulate green roof  
 211 performances at an annual time scale as a function of only two climatic variables (i.e.  $\bar{P}$  and  $\overline{ET_p}$ )  
 212 while keeping the problem as simple as possible. In order to do that, it is worth noting that the same  
 213 expected annual precipitation  $\bar{P}$  [mm/year] can be obtained by the infinite combination of  $\bar{\alpha}$  and  $\bar{\lambda}$ ,  
 214 as shown e.g. in Figure 1. Thus we decided to keep constant the mean interarrival time  $\bar{\lambda}$  for all the

215 simulated climatic conditions while exploring the variability of  $\bar{\alpha}$ ; consequently, different values of  
216  $\bar{P}$  will be obtained using the stochastic model of equations (1) and (2).

217 In order to apply our model with a reliable parametrization in different climatic conditions, we  
218 explored the parameter space by fitting Equations (1)-(3) to observed time series downloaded by  
219 the GHCN (Global Historical Climatology Network, [https://www.ncdc.noaa.gov/oa/climate/ghcn-](https://www.ncdc.noaa.gov/oa/climate/ghcn-daily/)  
220 [daily/](https://www.ncdc.noaa.gov/oa/climate/ghcn-daily/)) database, which pooled daily climate data from land surface stations across the globe. We  
221 focused the attention on daily precipitation and temperature data, using the 10,000 stations with  
222 longest time series. The location of the selected stations is reported in Figure 2.

223 With reference to rainfall, daily data from each station have been first analyzed at a monthly  
224 time scale in order to determine the average rainfall amount  $\alpha$  on wet days, the mean number of  
225 occurrences and consequently the rate of the Poisson process  $1/\lambda$  (estimated as the number of rainy  
226 days divided by the days in the month). The average values  $\bar{\alpha}$  and  $\bar{\lambda}$  have been thus estimated as the  
227 arithmetic mean from the monthly time series. For each year, the semi-amplitudes of the annual  
228 harmonic of  $\alpha$  and  $\lambda$  have been computed as the half of the difference between maximum and  
229 minimum values assumed at a monthly time scale. Parameters  $\delta_\lambda$  and  $\delta_\alpha$  have been finally  
230 estimated as the ratio between the mean of semi-amplitudes over all years and annual averages  $\bar{\alpha}$   
231 and  $\bar{\lambda}$ . Estimated parameters  $\bar{\lambda}$ ,  $\delta_\lambda$ ,  $\bar{\alpha}$ ,  $\delta_\alpha$ , for all the 10,000 considered stations, have been reported  
232 as histograms in Figure 3a, b, c, d.

233 Daily temperature data have been used to obtain potential evapotranspiration also taking into  
234 account solar insolation at the selected stations. Specifically, for each station, temperature  
235 observations have been averaged at a monthly time scale and then a monthly  $ET_p$  time series has  
236 been assessed by a simplified procedure as a function of temperature and station latitude  
237 (Thornthwaite, 1948). Similarly to eq. (1) and (2), for parameterization of eq. (3) average value  $\overline{ET_p}$   
238 has been estimated as the mean of monthly  $ET_p$  time series in each station, while the standardized  
239 semi-amplitude  $\delta_E$  has been estimated as the ratio between the mean of semi-amplitudes over all

240 years and annual average  $\overline{ET_p}$ . Figure 3e shows annual averages  $\overline{ET_p}$  obtained in the selected  
241 locations and reveals a quite symmetric distribution, while the standardized semi-amplitude  $\delta_E$  of  
242 the annual harmonic is shown in Figure 3f.

243 As anticipated, we decided to keep  $\bar{\lambda}$  constant for all simulations in order to keep the degree of  
244 freedom of the problem low. On the basis of our investigations, we assumed  $\bar{\lambda}$  equal to 4.35 days,  
245 that is the median value observed in the 10,000 considered stations (Figure 3a). We then considered  
246 five representative climatic regimes, hereafter named also cases, keeping constant rainfall rates and  
247 potential evapotranspiration during the hydrological year, or only one of the two, or considering  
248 both cyclic (in phase or in counter-phase). With the same intention to keep our set up simple, cyclic  
249 time series have been built keeping constant also the standardized semi-amplitudes of  $\lambda$ ,  $\alpha$  and  $ET_p$ ,  
250 that have been chosen as the median of their empirical distributions, i.e.  $\delta_\lambda = 0.45$ ,  $\delta_\alpha = 0.35$ ,  $\delta_E =$   
251  $0.30$ . Estimated parameters have been summarized in Table 1, where they are combined in order to  
252 depict five different climatic regimes.

253 The weather generator has been used to generate a 100-year-long rainfall and potential  
254 evapotranspiration daily time series for all the possible combinations of  $\bar{\alpha}$  and  $\overline{ET_p}$  for each  
255 climatic regime. Time series have been used as input to the conceptual hydrological model,  
256 discussed below.

257

## 258 **2.2 Runoff model**

259 The hydrological conceptual model introduced by Viola et al. (2014) has been used in order to  
260 simulate soil moisture dynamics in the soil layer and consequently an evapotranspirative flux and  
261 runoff from green roofs. Although the model has been developed for natural river basins, slight  
262 changes allow the conceptual scheme to be adapted to our setting, following a similar approach as

263 in former studies that applied conceptual models for simulating the hydrological behaviour of green  
 264 roofs (Palla et al., 2012).

265 Three interconnected elements have been used: a soil bucket linked with two linear reservoirs,  
 266 one accounting for the surface runoff component over the roofs, and another accounting for the  
 267 leakage collection and restitution. The runoff contribution per unit area has been calculated at a  
 268 daily time scale, considering the sewer connection as the basin outlet. The runoff over the green  
 269 roofs, although they are usually designed to limit and possibly avoid it, has been modelled by  
 270 saturation excess and then transferred to the sewer system through the surface reservoir with a  
 271 transit time of a day. Water leaked from the top soil layer is ideally collected by a second reservoir  
 272 characterized again by a residence time of one day. It is worth mentioning that although both the  
 273 transit and residence times are certainly less than one day, they are both set to one day according to  
 274 the time step of the adopted models.

275 The water input to the system is the daily rainfall depth,  $R$  [mm/day], which drives the relative  
 276 soil moisture dynamics. Soil is characterized by porosity and by root depth, termed  $n$  and  $Z_r$   
 277 respectively, whose product, known also as “active soil depth”, will be used as a model parameter.  
 278 The numerical solution of a simple balance equation, through a forward finite differences method,  
 279 allows the calculation of soil moisture variation within the soil bucket during a daily temporal step.  
 280 The runoff over the green roof ( $Q_s$ ) occurs when rainfall exceeds the available storage capacity and  
 281 is equal to the excess. The water losses due to evapotranspiration  $ET$  and leakage  $L = (s - s_t)nZ_r$  are  
 282 calculated at each time step as a function of the relative soil moisture ( $s$ ) as follows:

$$283 \quad ET + L = \begin{cases} 0 & \text{if } s \leq s_0 \\ ET_p \left( \frac{s - s_0}{s_t - s_0} \right) & \text{if } s_0 < s \leq s_t \\ ET_p + (s - s_t)nZ_r & \text{if } s_t < s \leq 1 \end{cases} \quad (4)$$

284 where  $s_t$  has a role of field capacity and  $s_0$  represents the wilting point. The evapotranspiration-  
 285 leakage-soil moisture relation is modelled assuming that when relative soil moisture exceeds  $s_t$ ,

286 evapotranspiration occurs at the maximum rate,  $ET_p$ , while saturation water  $(s - s_t)nZ_r$  is  
287 transferred instantaneously to the conceptual linear reservoir. Below  $s_t$ , no leakage occurs and  
288 evapotranspiration decreases linearly to zero for relative soil moisture equal to  $s_0$  or less. As already  
289 pointed out by Viola et al. (2016), the relation in eq.(4) between the soil moisture and water losses  
290 is simple and parsimonious because it uses only three parameters, two characterizing the soil  
291 properties ( $s_t$  and  $s_0$ ) and one representing the maximum (or potential) evapotranspiration rate  $ET_p$ .  
292 In order to take into account the influence of vegetation on water demand, a vegetational coefficient  
293 should be introduced. However, the virtual vegetation variability (as defined e.g. by Viola et al.  
294 (2014)) would introduce another degree of complexity to the problem; thus we preferred to consider  
295 a single vegetation type that will be used for both intensive and extensive green roofs.

296 The total runoff  $Q$  is simply computed as the sum of two contributions: the excess saturation  
297 surface runoff,  $Q_s$ , and the leakage,  $L$ . Each contribution is routed into a linear reservoir  
298 characterized by a one-day residence time.

299 Model outputs have been aggregated at a yearly time scale and then averaged to estimate an  
300 index of retention (IOR) defined as the ratio between actual evapotranspiration and rainfall for each  
301 100-year-long time series. This index can range between zero (no evapotranspiration, green roofs  
302 are ineffective) and one (all the rain is diverted into evapotranspiration, thus the green roof has a  
303 perfect efficiency in reducing water inputs to the sewer system). The IOR has been calculated in the  
304 five representative climatic regimes, introduced in section 2.1, and referring to two green roof  
305 configurations. The first is an extensive one, thus a thin layer of active soil (depth of 90 mm), while  
306 the second is an intensive configuration characterized by a deeper soil ( $nZ_r = 450$  mm). Both the  
307 analyzed configurations have the same soil hydrological properties and same vegetation; thus the  
308 same parameters  $s_0 = 0.30$  and  $s_t = 0.85$  have been adopted in eq.(4) for both configurations.

309

### 310 **3. Results**

311 Each of the proposed representative climatic regimes, introduced in section 2.1, refers to a  
312 specific combination of rainfall and potential evapotranspiration during the hydrological year. For  
313 each case the influence of annual rainfall  $P$  (ranging from zero to 3000 mm/year) and potential  
314 evapotranspiration  $ET_p$  (ranging from zero to 2000 mm/year) in leading to annual water retention is  
315 explored with reference to extensive ( $nZ_r = 90$  mm) and intensive ( $nZ_r = 450$  mm) green roof  
316 configurations, and performances evaluated in terms of IOR for all the possible  $P$ - $ET_p$   
317 combinations are presented in Figure 4.

318 Table 1 reports the averages of the obtained IORs within the chosen domain of rainfall and  
319 potential evapotranspiration, in order to give an indicative performance score that is helpful in  
320 comparing the five representative climatic regimes,. Furthermore 25 cities have been proposed as  
321 benchmark examples. Each of these cities has been attributed to a given climatic case and from  
322 graphical analysis of Figure 4 it is possible to argue about green roof retention performances, for  
323 both intensive and extensive configurations, in those selected locations.

324 The first analyzed case refers to stationary conditions that can be considered as an ideal  
325 reference condition: rainfall statistics are supposed to remain unaltered within the hydrological year  
326 as well as potential evapotranspiration. Figure 4, central and right subplots in the first row, presents  
327 results in terms of IOR for the two analyzed soil configurations. The average retention observed for  
328 all the possible combinations of annual rainfall and potential evapotranspiration is 52.8% for the  
329 thin soil and 59.6% for the deep soil, confirming that intensive configurations are more effective in  
330 retaining water. This is obviously due to the higher active soil depth, which can store more water,  
331 reducing deep leakages and consequently allowing more water evaporation from soil and  
332 vegetation.

333 The second case is representative of zones where rainfall is almost constant during the  
334 hydrological year, but temperature and consequently potential evapotranspiration have one peak as  
335 it is, for instance, in oceanic climate. The green roof performances in these climatic conditions are

336 comparable to those obtained in the steady state case (see Table 1), results in terms of IOR for the  
337 two analyzed configurations are shown in Figure 4, second row. The city of New York falls in this  
338 climatic case: in fact the monthly rainfall is almost constant during the year (about 100 mm/month),  
339 while temperatures show seasonality, with a peak during the summer (about 23 °C in August) and a  
340 trough in winter (about 0° in January). From Figure 4 it is possible to extract the mean retention  
341 efficiency for extensive (i.e. IOR = 0.55) and intensive configuration (i.e. IOR = 0.62) for this city.

342 In the third case we summarized world areas where potential evapotranspiration could be  
343 considered constant through the hydrological year while rainfall shows seasonal patterns with one  
344 peak. This is the case for tropical climates. Retention performances in this case decrease: the  
345 average percentage of rainfall diverted into evapotranspiration is 49.9% for extensive green roofs  
346 and 57.2% for the intensive ones (see Table 1). This drop in performances, with respect to the ideal  
347 case 1, is explained by more runoff and leakage produced during the heavy rainfall periods. Results  
348 are shown in Figure 4, third row, and the city of Mumbai could be presented as the paradigm of this  
349 climatic situation. Temperature is almost constant during the year (27°C as daily mean), but rainfall  
350 is mostly concentrated during the monsoon period (from June to September). In this city, with this  
351 peculiar climate, the mean retention efficiency for intensive green roofs is equal to 0.34 while for  
352 extensive configurations is 0.41.

353 The world areas where both rainfall and temperature display seasonal cycles have been  
354 summarized in the last two cases. In case 4 we consider in-phase climatic forcings, meaning that  
355 when rain is high, the evapotranspiration demand is high, too. Such a condition occurs in humid  
356 subtropical climates. Performances in this case are again comparable with the ideal case 1 (see  
357 Table 1). Indeed when rainfall inputs increase also losses due to evapotranspiration increase,  
358 keeping soil moisture dynamics similar to those observed in the case 1. Figure 4, fourth row,  
359 depicts the IOR for all the explored combinations of annual rainfall and potential  
360 evapotranspiration for the two green roof configurations. Tokyo is one of the cities belonging to  
361 this case: the analysis of climatic statistics shows how the temperature has a seasonal behaviour,

362 with a peak in August (average daily mean of about 23°C) when rainfall has its maximum (about  
363 280 mm/month). Results for this city reveal that extensive green roofs retain 48% of annual rainfall,  
364 while intensive ones retain 56%.

365 The last case refers to areas where rainfall and potential evapotranspiration are in counter-phase  
366 during the hydrological year, as happens with a Mediterranean climate. This climatic condition is  
367 the worst in terms of retention performances, that are the lowest among the analyzed cases (0.47 for  
368 extensive and 0.54 for intensive green roofs). The physical explanation for more runoff occurring in  
369 such a climate is that when potential evapotranspiration is low, rainfall saturates the soil triggering  
370 leakage and superficial runoff. Results are shown in Table 1 and Figure 4, fifth row. Among the  
371 analyzed cities, Rome with hot summers (25 °C of daily mean in August) and mild rainy winters  
372 (with more than 80% of rain falling from October to April), falls in this latter climatic case.

373 To give evidence of the reliable results provided by the design charts plotted in Figure 4, and  
374 thus also of the overall good performances of the modelling approach adopted in this study, we  
375 refer to the results presented by Stovin et al. (2013) and Carson et al. (2013), already described in  
376 the introduction. Namely, we compared the index of retention as obtained by the mentioned authors  
377 with those provided by our design charts in Figure 4. In particular, we first attributed each location  
378 studied in Stovin et al. (2013) and Carson et al. (2013) to a climatic case, and then extrapolated the  
379 main climatic conditions (i.e. mean annual rainfall and potential annual evapotranspiration) which  
380 determined the performances of the analyzed green roofs. Then, we used the design charts in Figure  
381 4 to calculate the IOR, referring to intensive or extensive configurations depending on the  
382 considered case study. Results of these comparisons, which have been reported in Table 2, show a  
383 good accordance in very different climatic conditions, with negligible discrepancies between  
384 observations and modelled IORs which are mainly imputable to the different soil capacity  
385 considered and can certainly be accepted under the assumptions and simplifications here made.

386

#### 387 **4. Conclusion**

388 A worldwide assessment of retention efficiency of green roofs has been carried out and  
389 presented in this study with the aim to provide information to scientists, practitioners and policy  
390 makers involved in urban planning and interested in evaluating the possible hydrological impact of  
391 green roofs in areas where this evaluation is tricky or impossible, due e.g. to the lack of climatic  
392 data (rainfall and temperature) or the costs of field experiments. Specifically we designed a tool for  
393 a first-approximate estimate of green roof retention performances in different climates with respect  
394 to intensive and extensive configurations, by coupling a simple stochastic weather generator with a  
395 conceptual model miming the hydrological behaviour of the green roof. Massive numerical  
396 simulations have been carried out in order to generate rainfall and potential evapotranspiration time  
397 series in different climates and afterwards to evaluate hydrological water fluxes through the two  
398 green roof configurations.

399 Results highlight the role of soil depth and climate in driving the retention capacity of a green  
400 roof. The amount of retained water increases with increasing soil depth, because more water is  
401 allowed to be stored in the active soil and consequently more water can evaporate from soil and  
402 vegetation. Regarding the climate, the performance of a green roof increases when rainfall and  
403 potential evapotranspiration exhibit the same seasonality during the hydrological year (i.e. their  
404 forcings are in-phase), as happens, for example in humid subtropical climates. Conversely, the  
405 green roof presents the minimum efficiency when rainfall and potential evapotranspiration are in  
406 counter-phase, as is found in a Mediterranean climate.

407 Moreover, we provided design charts for representative climates worldwide, which make it  
408 possible to evaluate quickly green roof performances starting from easy-to-obtain data and climatic  
409 information. Monthly rainfall and temperature distribution will guide the user in the choice of the  
410 appropriate climatic case as a function of rainfall and temperature stationarity or seasonality within  
411 a generic hydrological year. Then the annual mean value of rainfall and potential

412 evapotranspiration are the only required data in order to evaluate how much water is retained by the  
413 green roof system, or conversely how much is released into the stormwater sewer system. Two  
414 main green roof configurations have been explored, intensive and extensive: for both an evaluation  
415 of the index of retention (ranging from 0, when all the rainfall is turned into runoff, to 1, when all  
416 the rainfall is retained and evapotranspired) can be read from the corresponding design charts.

417 Further research efforts are needed in order to examine the role of rainfall extremes in driving  
418 green roof retention and detection performances at temporal time scales shorter than a day, which  
419 are crucial for sewer system design. This will be challenging for the complexity of extreme rainfall  
420 statistics depending not only on site location but also on local conditions as topography or sea  
421 distance.

422

## 423 **Acknowledgments**

424 This work has been partially funded by *Regione Siciliana – Dipartimento Attività Produttive,*  
425 *“PO FESR 2007-2013”.* *“Linea di intervento 4.1.2.a.: Azioni di qualificazione dell’offerta di*  
426 *ricerca e servizi a supporto all’innovazione e al trasferimento tecnologico (Qualification research*  
427 *actions and services to support innovation and technology transfer)”.* Project: *“Rete Integrata dei*  
428 *Laboratori Tecnologici delle Università Siciliane – RILTUS”.*

429

430

431 **References**

- 432 Bengtsson, L., Grahn, L., Olsson, J., 2005. Hydrological function of a thin extensive green roof  
433 in southern Sweden. *Nordic Hydrology*, 36(3): 259-268.
- 434 Berardi, U., Ghaffarian Hoseini, A., 2014. State-of-the-art analysis of the environmental  
435 benefits of green roofs. *Applied Energy*, 115: 411-428.  
436 DOI:10.1016/j.apenergy.2013.10.047
- 437 Burlando, P., Rosso, R., 1991. Comment on “Parameter estimation and sensitivity analysis for  
438 the modified Bartlett-Lewis rectangular pulses model of rainfall” by S. Islam et al.  
439 *Journal of Geophysical Research: Atmospheres*, 96(D5): 9391-9395.
- 440 Carson, T.B., Marasco, D.E., Culligan, P.J., McGillis, W.R., 2013. Hydrological performance of  
441 extensive green roofs in New York City: Observations and multi-year modeling of three  
442 full-scale systems. *Environmental Research Letters*, 8(2). DOI:10.1088/1748-  
443 9326/8/2/024036
- 444 Carter, T., Jackson, C.R., 2007. Vegetated roofs for stormwater management at multiple spatial  
445 scales. *Landscape and Urban Planning*, 80(1-2): 84-94.  
446 DOI:10.1016/j.landurbplan.2006.06.005
- 447 Carter, T.L., Rasmussen, T.C., 2006. Hydrologic behavior of vegetated roofs. *Journal of the*  
448 *American Water Resources Association*, 42(5): 1261-1274.
- 449 Cipolla, S.S., Maglionico, M., Stojkov, I., 2016. A long-term hydrological modelling of an  
450 extensive green roof by means of SWMM. *Ecological Engineering*, 95: 876-887.  
451 DOI:10.1016/j.ecoleng.2016.07.009
- 452 Cowpertwait, P., Kilsby, C., O'Connell, P., 2002. A space-time Neyman-Scott model of rainfall:  
453 Empirical analysis of extremes. *Water Resources Research*, 38(8).
- 454 Cowpertwait, P., O'Connell, P., Metcalfe, A., Mawdsley, J., 1996. Stochastic point process  
455 modelling of rainfall. I. Single-site fitting and validation. *Journal of Hydrology*, 175(1-  
456 4): 17-46.
- 457 Cowpertwait, P.S., 1991. Further developments of the Neyman-Scott clustered point process for  
458 modeling rainfall. *Water Resources Research*, 27(7): 1431-1438.
- 459 Cowpertwait, P.S., O'Connell, P.E., 1997. A regionalised Neyman-Scott model of rainfall with  
460 convective and stratiform cells. *Hydrology and Earth System Sciences Discussions*,  
461 1(1): 71-80.
- 462 Czemieli Berndtsson, J., 2010. Green roof performance towards management of runoff water  
463 quantity and quality: A review. *Ecological Engineering*, 36(4): 351-360.  
464 DOI:10.1016/j.ecoleng.2009.12.014
- 465 DeNardo, J.C., Jarrett, A.R., Manbeck, H.B., Beattie, D.J., Berghage, R.D., 2005. Stormwater  
466 mitigation and surface temperature reduction by green roofs. *Transactions of the*  
467 *American Society of Agricultural Engineers*, 48(4): 1491-1496.
- 468 Dietz, M.E., 2007. Low impact development practices: A review of current research and  
469 recommendations for future directions. *Water, Air, and Soil Pollution*, 186(1-4): 351-  
470 363. DOI:10.1007/s11270-007-9484-z
- 471 Dvorak, B., Volder, A., 2010. Green roof vegetation for North American ecoregions: A  
472 literature review. *Landscape and Urban Planning*, 96(4): 197-213.  
473 DOI:10.1016/j.landurbplan.2010.04.009

- 474 Entekhabi, D., Rodriguez-Iturbe, I., Eagleson, P.S., 1989. Probabilistic representation of the  
475 temporal rainfall process by a modified Neyman-Scott Rectangular Pulses Model:  
476 Parameter estimation and validation. *Water Resources Research*, 25(2): 295-302.
- 477 Feng, C., Meng, Q., Zhang, Y., 2010. Theoretical and experimental analysis of the energy  
478 balance of extensive green roofs. *Energy and Buildings*, 42(6): 959-965.  
479 DOI:10.1016/j.enbuild.2009.12.014
- 480 Fioretti, R., Palla, A., Lanza, L.G., Principi, P., 2010. Green roof energy and water related  
481 performance in the Mediterranean climate. *Building and Environment*, 45(8): 1890-  
482 1904. DOI:10.1016/j.buildenv.2010.03.001
- 483 Getter, K.L., Rowe, D.B., 2006. The role of extensive green roofs in sustainable development.  
484 *HortScience*, 41(5): 1276-1285.
- 485 Getter, K.L., Rowe, D.B., Andresen, J.A., 2007. Quantifying the effect of slope on extensive  
486 green roof stormwater retention. *Ecological Engineering*, 31(4): 225-231.  
487 DOI:10.1016/j.ecoleng.2007.06.004
- 488 Hilten, R.N., Lawrence, T.M., Tollner, E.W., 2008. Modeling stormwater runoff from green  
489 roofs with HYDRUS-1D. *Journal of Hydrology*, 358(3-4): 288-293.  
490 DOI:10.1016/j.jhydrol.2008.06.010
- 491 Islam, S., Entekhabi, D., Bras, R., Rodriguez-Iturbe, I., 1990. Parameter estimation and  
492 sensitivity analysis for the modified Bartlett-Lewis rectangular pulses model of rainfall.  
493 *Journal of Geophysical Research: Atmospheres*, 95(D3): 2093-2100.
- 494 Laio, F., Porporato, A., Ridolfi, L., Rodriguez-Iturbe, I., 2001. Plants in water-controlled  
495 ecosystems: active role in hydrologic processes and response to water stress: II.  
496 Probabilistic soil moisture dynamics. *Advances in Water Resources*, 24(7): 707-723.
- 497 Locatelli, L. et al., 2014. Modelling of green roof hydrological performance for urban drainage  
498 applications. *Journal of Hydrology*, 519(PD): 3237-3248.  
499 DOI:10.1016/j.jhydrol.2014.10.030
- 500 Milly, P.C.D., 1994. Climate, soil water storage, and the average annual water balance. *Water*  
501 *Resources Research*, 30(7): 2143-2156. DOI:10.1029/94wr00586
- 502 Monterusso, M.A., Rowe, D.B., Rugh, C.L., Russell, D.K., 2004. Runoff water quantity and  
503 quality from green roof systems, *Acta Horticulturae*, pp. 369-376.
- 504 Palla, A., Gnecco, I., Lanza, L.G., 2009. Unsaturated 2D modelling of subsurface water flow in  
505 the coarse-grained porous matrix of a green roof. *Journal of Hydrology*, 379(1-2): 193-  
506 204. DOI:10.1016/j.jhydrol.2009.10.008
- 507 Palla, A., Gnecco, I., Lanza, L.G., 2012. Compared performance of a conceptual and a  
508 mechanistic hydrologic models of a green roof. *Hydrological Processes*, 26(1): 73-84.  
509 DOI:10.1002/hyp.8112
- 510 Puente, C., Bierkens, M., Diaz-Granados, M., Dik, P., López, M., 1993. Practical use of  
511 analytically derived runoff models based on rainfall point processes. *Water Resources*  
512 *Research*, 29(10): 3551-3560.
- 513 Rodriguez-Iturbe, I., Cox, D., Isham, V., 1987a. Some models for rainfall based on stochastic  
514 point processes, *Proceedings of the Royal Society of London A: Mathematical, Physical*  
515 *and Engineering Sciences*. The Royal Society, pp. 269-288.
- 516 Rodríguez-Iturbe, I., Power, B.F., Valdes, J.B., 1987b. Rectangular pulses point process models  
517 for rainfall: analysis of empirical data. *Journal of Geophysical Research: Atmospheres*,  
518 92(D8): 9645-9656.

519 Šimůnek, J., van Genuchten, M.T., Šejna, M., 2008. Development and applications of the  
520 HYDRUS and STANMOD software packages and related codes. *Vadose Zone Journal*,  
521 7(2): 587-600.

522 Stovin, V., 2010. The potential of green roofs to manage urban stormwater. *Water and*  
523 *Environment Journal*, 24(3): 192-199. DOI:10.1111/j.1747-6593.2009.00174.x

524 Stovin, V., Poë, S., Berretta, C., 2013. A modelling study of long term green roof retention  
525 performance. *Journal of Environmental Management*, 131: 206-215.  
526 DOI:10.1016/j.jenvman.2013.09.026

527 Stovin, V., Vesuviano, G., Kasmin, H., 2012. The hydrological performance of a green roof test  
528 bed under UK climatic conditions. *Journal of Hydrology*, 414-415: 148-161.  
529 DOI:10.1016/j.jhydrol.2011.10.022

530 Thornthwaite, C.W., 1948. An approach toward a rational classification of climate.  
531 *Geographical review*, 38(1): 55-94.

532 Verhoest, N., Troch, P.A., De Troch, F.P., 1997. On the applicability of Bartlett–Lewis  
533 rectangular pulses models in the modeling of design storms at a point. *Journal of*  
534 *Hydrology*, 202(1): 108-120.

535 Viola, F. et al., 2016. Co-evolution of hydrological components under climate change scenarios  
536 in the Mediterranean area. *Science of the Total Environment*, 544: 515-524.  
537 DOI:10.1016/j.scitotenv.2015.12.004

538 Viola, F., Pumo, D., Noto, L.V., 2014. EHSM: A conceptual ecohydrological model for daily  
539 streamflow simulation. *Hydrological Processes*, 28(9): 3361-3372.

540 Voyde, E., Fassman, E., Simcock, R., 2010. Hydrology of an extensive living roof under sub-  
541 tropical climate conditions in Auckland, New Zealand. *Journal of Hydrology*, 394(3-4):  
542 384-395. DOI:10.1016/j.jhydrol.2010.09.013

543 Wilby, R.L., 1999. The weather generation game: A review of stochastic weather models.  
544 *Progress in Physical Geography*, 23(3): 329-357.

545

546

547

548 **Table**

|               | $\lambda(t)$              |                         |                           | $\alpha(t)$                 |                        |                          | $ET_p(t)$                      |                   |                     | Index Of Retention |               |
|---------------|---------------------------|-------------------------|---------------------------|-----------------------------|------------------------|--------------------------|--------------------------------|-------------------|---------------------|--------------------|---------------|
|               | $\bar{\lambda}$<br>[days] | $\delta_\lambda$<br>[-] | $\omega_\lambda$<br>[rad] | $\bar{\alpha}$<br>[mm/days] | $\delta_\alpha$<br>[-] | $\omega_\alpha$<br>[rad] | $\overline{ET_p}$<br>[mm/days] | $\delta_E$<br>[-] | $\omega_E$<br>[rad] | nZr<br>90 mm       | nZr<br>450 mm |
| <b>Case 1</b> | 4.35                      | 0                       | 0                         | Variable                    | 0                      | 0                        | variable                       | 0                 | 0                   | 0.529              | 0.596         |
| <b>Case 2</b> | 4.35                      | 0                       | 0                         | Variable                    | 0                      | 0                        | variable                       | 0.30              | $-\pi/2$            | 0.518              | 0.590         |
| <b>Case 3</b> | 4.35                      | 0.45                    | $-\pi/2$                  | Variable                    | 0.35                   | $\pi/2$                  | variable                       | 0                 | 0                   | 0.500              | 0.572         |
| <b>Case 4</b> | 4.35                      | 0.45                    | $-\pi/2$                  | Variable                    | 0.35                   | $\pi/2$                  | variable                       | 0.30              | $\pi/2$             | 0.519              | 0.585         |
| <b>Case 5</b> | 4.35                      | 0.45                    | $-\pi/2$                  | Variable                    | 0.35                   | $\pi/2$                  | variable                       | 0.30              | $-\pi/2$            | 0.471              | 0.545         |

549

550 **Table 1:** Weather generator parameters used in equations (1) - (3) to simulate the five climatic  
 551 regimes and index of retention (IOR) for the two green roof configurations analyzed.

552

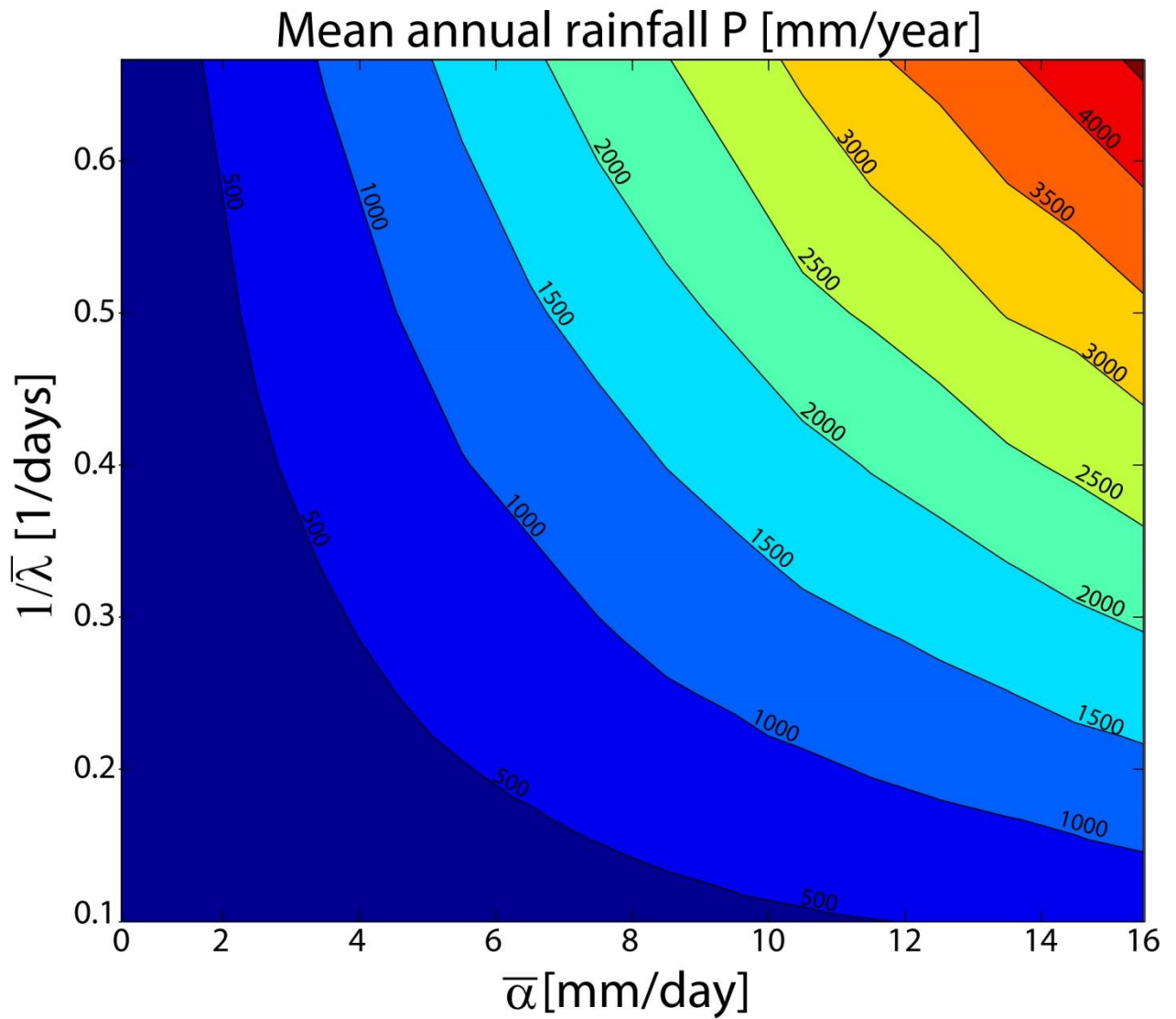
| <b>Location</b> | <b>Case (1-5)</b> | $\bar{P}$<br>[mm/year] | $\overline{ET_p}$<br>[mm/year] | <b>IOR</b><br>from Stovin et al. (2013)* and<br>Carson et al. (2013)** | <b>IOR</b><br>from Figure 4 |
|-----------------|-------------------|------------------------|--------------------------------|--|-----------------------------|
| NW Scotland     | 5                 | 2700                   | 620                            | 0.19*  | 0.2                         |
| Sheffield       | 5                 | 838                    | 670                            | 0.40*  | 0.5                         |
| Cornwall        | 5                 | 1360                   | 650                            | 0.33*  | 0.4                         |
| East Midlands   | 2                 | 500                    | 700                            | 0.59*  | 0.74                        |
| New York        | 2                 | 1290                   | 750                            | 0.58**   | 0.55                        |

553 **Table 2:** Comparison of green roof retention performances as resulted from literature studies and  
554 from the design charts given in Figure 4.

555

556

557 **Figures**

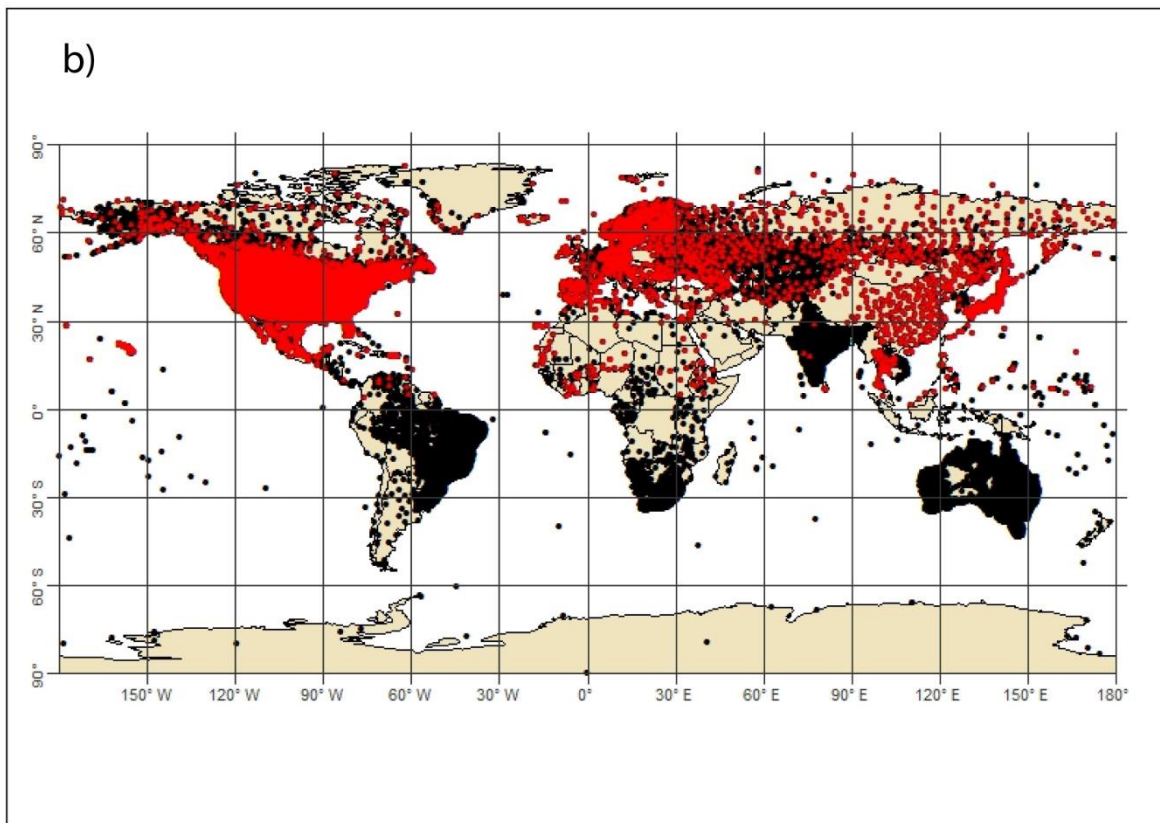
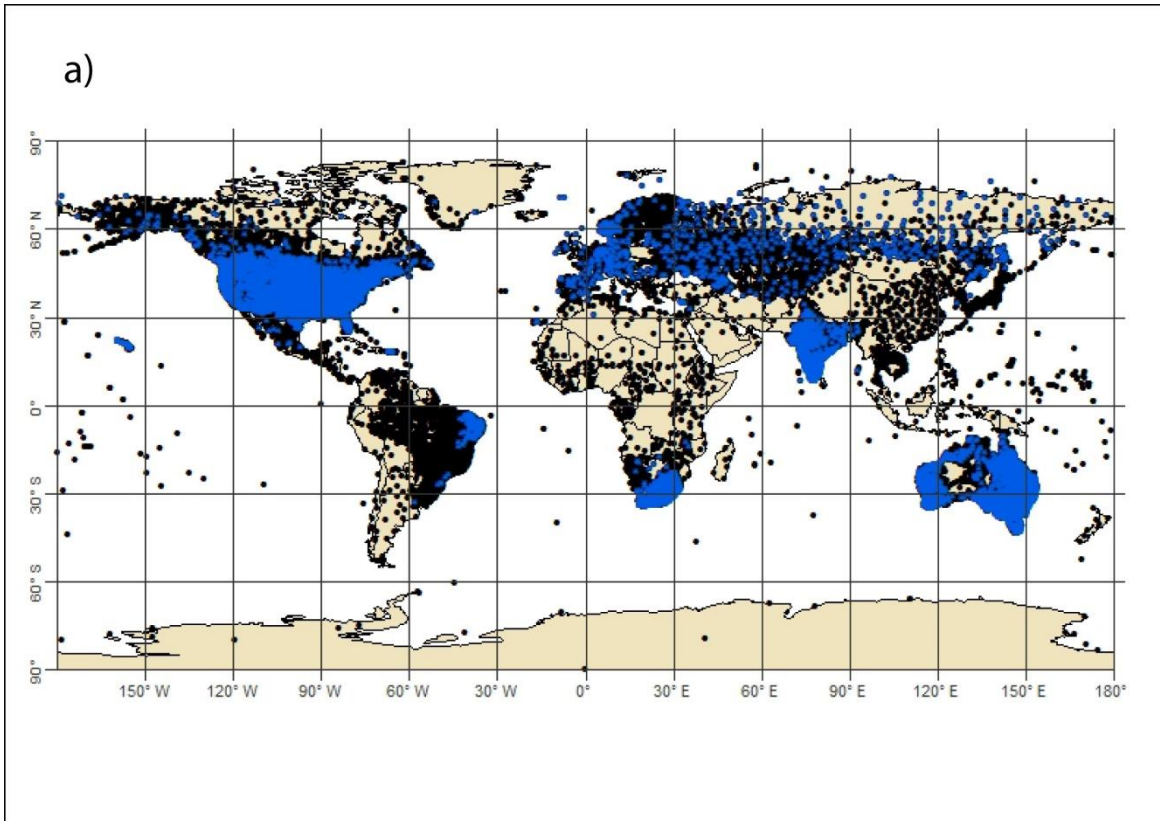


558

559 **Figure 1:** Expected annual rainfall depths as a function of average interarrival time  $\bar{\lambda}$  and  
560 average amount of rainfall  $\bar{\alpha}$  as obtained by integration of equations. (1) and (2) with parameters  
561  $\delta_\lambda=0.45$ ;  $\delta_\alpha=0.35$ ;  $\omega_\lambda=-\pi/2$ ;  $\omega_\alpha=\pi/2$ .

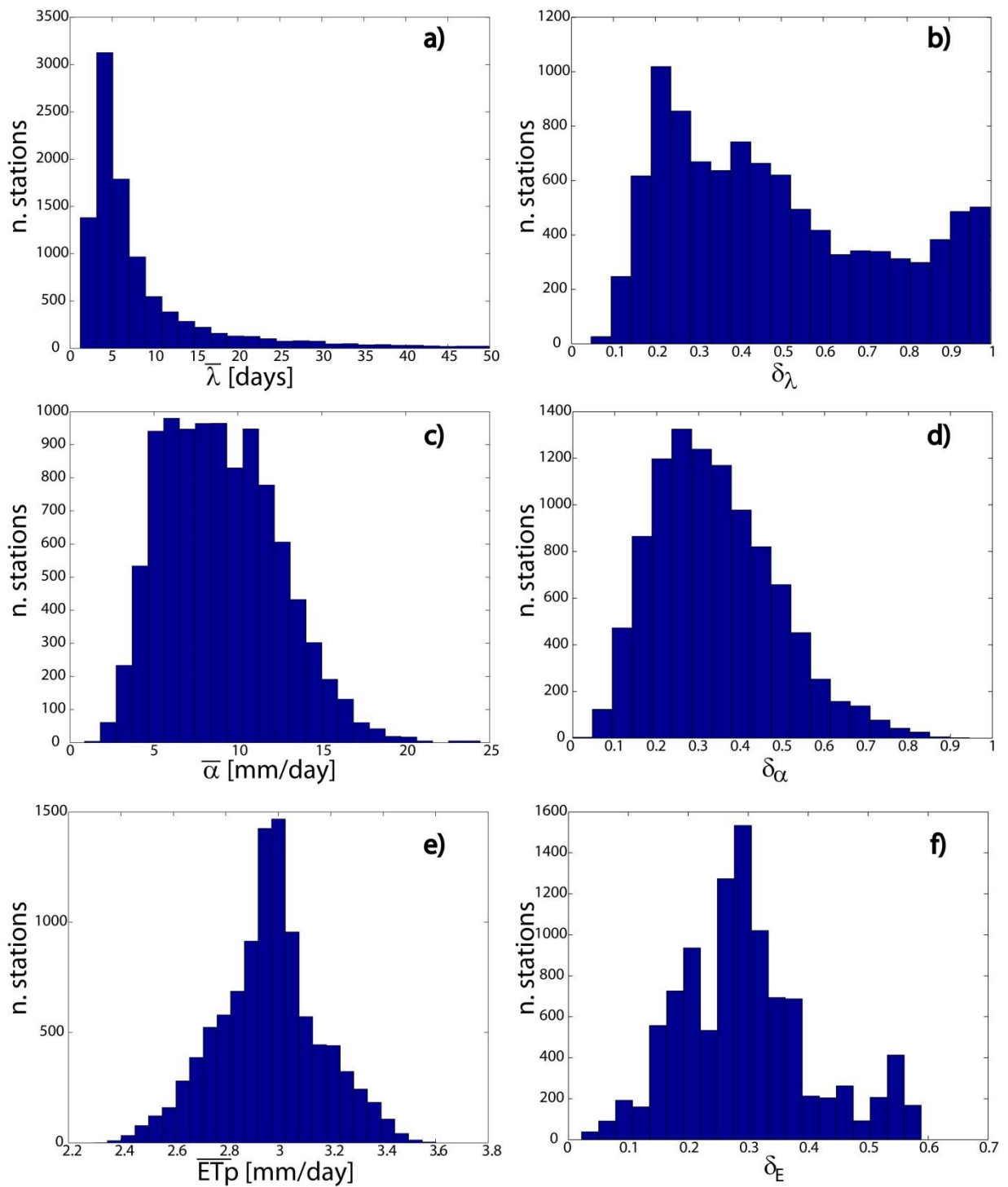
562

563



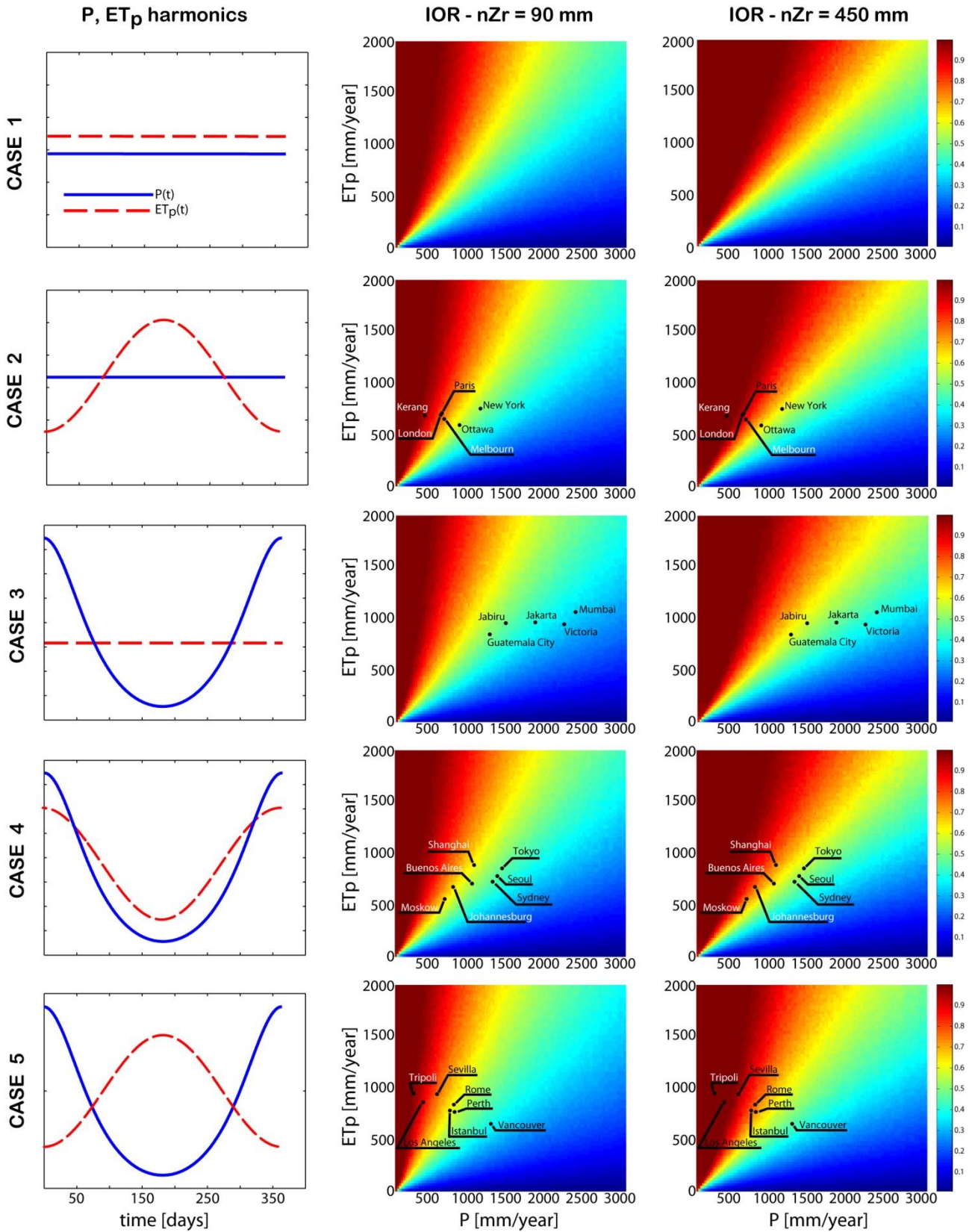
564

565 **Figure 2:** Location of the 10,000 rainfall (a) and temperature (b) gauging stations used to  
 566 parameterize the weather generator (Data from <https://www.ncdc.noaa.gov/oa/climate/ghcn-daily>)



568

569 **Figure 3:** Worldwide statistics from the 10,000 selected stations for: average rainfall interarrival  
 570 time  $\bar{\lambda}$  (a) and corresponding standardized semi-amplitude  $\delta_\lambda$  (b); average amount of rainfall  $\bar{\alpha}$  (c)  
 571 and corresponding standardized semi-amplitude  $\delta_\alpha$  (d); average potential evapotranspiration  $\overline{ET}_p$   
 572 (e) and corresponding standardized semi-amplitude  $\delta_E$  (f).



574

575 **Figure 4:** Green roof retention performances in different climates (first column) and for two  
 576 active soil depths: second column refers to extensive configurations (i.e.  $nZ_r = 90\text{mm}$ ) while the

577 third column refers to intensive configurations (i.e.  $nZ_r = 450\text{mm}$ ). Results are shown in terms of  
578 index of retention IOR ( $\overline{ET}/\overline{P}$ ), as a function of mean annual rainfall  $\overline{P}$  and mean annual potential  
579 evapotranspiration  $\overline{ET}_p$ . Dots indicate climatic conditions for selected large cities, to show the  
580 simple usage of the design charts for estimation of green roof performances.

581

582